Architectural Effects of Poly(ϵ-caprolactone)s on the Crystallization Kinetics

Jeongsoo Choi[†] and Seung-Yeop Kwak*[,‡]

Research Institute of Advanced Materials (RIAM), and School of Materials Science and Engineering, Seoul National University, San 56-1, Shinlim-dong, Kwanak-ku, Seoul 151-744, Korea, and Hyperstructured Organic Materials Research Center (HOMRC), and School of Materials Science and Engineering, Seoul National University, San 56-1, Shinlim-dong, Kwanak-ku, Seoul 151-744, Korea

Received September 17, 2003; Revised Manuscript Received February 12, 2004

ABSTRACT: A series of hyperbranched poly(ϵ-caprolactone)s (HPCLs) with molecular architectural variation, which refers to the different lengths of the linear backbone segments consisting of 5, 10, and 20 ϵ-caprolactone monomer units (thereby referred to as HPCL-5, HPCL-10, and HPCL-20, respectively) and the different numbers of branching points, were synthesized without significant variation in the molecular weights, and linear poly(ϵ-caprolactone) (LPCL) of the same chemical structure and similar molecular weight was used as the linear counterpart to HPCLs for comparison. The specific molecular architectures of these samples were characterized by ^{1}H NMR end-group analyses. The nonisothermal crystallization exotherms of HPCLs and LPCL were measured by DSC and further analyzed by the modified Avrami method. Regardless of the samples, the Avrami exponents ranged from 2.4 to 3.3, indicating that the nucleation and growth mechanisms of the samples are apparently identical. On the other hand, the crystallization kinetics was found to be fairly affected by the molecular architectures. All the kinetic parameters estimated from DSC exotherms such as the initial slope, S_i, and from the modified Avrami analyses such as the corrected rate constant, K_c, and crystallization half-time, $t_{1/2}$, indicated that HPCLs with longer linear segments and fewer branches showed the faster crystallization, whereas LPCL exhibited intermediate crystallization rate between HPCL-10 and HPCL-20, i.e., HPCL-5 < HPCL-10 < LPCL < HPCL-20. The slower crystallization was linked with the frequent presence of heterogeneous branching points, hindering the regular chain packing, in the backbone of HPCLs with shorter linear segments. In addition, the faster crystallization of HPCL-20 compared with LPCL was attributed to the higher cooperative chain mobility in their melt state as evaluated by activation energy of flow. A number of spherulites developed during isothermal process from the melt were observed for all samples by POM, and the radial growth rates of these spherulites were evaluated to correspond well with the results of S_i, K_c, and $t_{1/2}$ from the nonisothermal crystallization analyses.

1. Introduction

Macromolecules possessing complex molecular architectures have received increasing attention during the past decade. This interest is governed by the realization that new and/or improved material properties can be obtained by altering the architecture of the polymers, which further enables development of tailor-made materials and to apply them to specific application where high performance and/or novel functionality are demanded.[1,2] One example in this context is the dendritic macromolecules, which are mainly classified into dendrimers with perfectly branched structure and hyperbranched polymers (HBPs) with statistically branched structure. Compared with dendrimers obtained from multistep syntheses,[3,4] HBPs are more advantageous for practical purposes since they can be easily synthesized through one-step polymerization of AB_x ($x \geq 2$) monomers.[5,6] Because of their highly functionalyzed globular architectures, HBPs exhibit different properties from those of their linear counterpart of the same molecular weight, such as less entanglement in the solid state,[1] high solubility in various solvents, low melt viscosity,[7−9] and fast molecular motion.[10,11] Although this attractive feature has led to the development of many different architectures involving a large number of building blocks,[12−17] it is difficult to tailor-make properties of HBPs since only a few parameters can be adjusted and/or modified.

Recently, several approaches to the development of HBPs or their derivatives with large versatilities through the preparation of block copolymers or through the introduction of controlled branching have been reported. Among these approaches, the synthesis of hyperbranched poly(ϵ-caprolactone) (HPCL) is quite noteworthy because this novel synthetic approach allows the production of a homologous series of HPCLs with a range of molecular architectural variation such as different lengths of linear backbone segments and different numbers of branching points.[18,19] However, to our knowledge, there is no detailed study on the correlation between these specific molecular architectures of HPCLs and the resulting material properties such as the crystallization behaviors.

The crystallization behaviors of polymeric materials have been typically studied through both the isothermal and the nonisothermal crystallization measurements.[20] Numerous studies have been reported concerning the different effects observed during the isothermal crystallization since the theoretical analysis of the isothermal crystallization data is relatively simple. In contrast, there are a comparatively limited number of publications dealing directly with a quantitative evaluation of the kinetic parameters for the nonisothermal crystal-

[†] Research Institute of Advanced Materials.
[‡] Hyperstructured Organic Materials Research Center.
* To whom correspondence should be addressed: e-mail sykwak@snu.ac.kr.

10.1021/ma035387f CCC: $27.50
Published on Web 04/15/2004

lization because the treatment of dynamic crystallization data is rather complicated.[21,22] However, it is without question that the study of the nonisothermal crystallization is of great practical importance since this type of crystallization approaches more closely to the industrial conditions of polymer processing such as extrusion, molding, melt spinning of synthetic fibers, among others.[23,24] In addition, a study dealing with the isothermal and/or nonisothermal crystallization behavior of the macromolecules possessing complex molecular architecture as well as the effects of the specific molecular architecture on the crystallization behavior is essential for designing new materials with novel properties.

In this study, a series of HPCLs were synthesized to incorporate various different lengths of linear homologous oligo(ϵ-caprolactone) backbone segments consisting of 5, 10, and 20 ϵ-caprolactone monomer units and are thereby referred to as HPCL-5, HPCL-10, and HPCL-20, respectively. The difference in the macromolecular architecture among HPCLs and LPCL was characterized by ^{1}H NMR end-group analyses. The controlled nonisothermal crystallization was performed with various cooling rates by DSC and analyzed by the modified Avrami method. Cooperative polymer chain mobility in the melt state was characterized from the steady-shear melt viscosity measurements, and the developed crystal morphology as well as the spherulites growth during isothermal process was observed using POM. The focal point of this study is characterizing the crystallization kinetics of HPCLs and LPCL in a rather quantitative and comparative manner and, consequently, elucidating the effects of the specific molecular architecture of HPCLs and LPCL on the crystallization kinetics.

2. Experiments

2.1. Materials. The initiator **1**, 2,2-bis(hydroxymethyl)-propyl benzoate, for ring-opening polymerization of ϵ-caprolactone was prepared by nucleophilic substitution of potassium salt of 2,2-bis(hydroxymethyl)propionic acid (bis-MPA) with benzyl bromide. Benzyl-protected AB_2 macromonomers **2**, 2,2-bis[ω-hydroxyoligo(ϵ-caprolactone)methyl]propyl benzoates, were prepared to incorporate the various lengths of oligo(ϵ-caprolactone) segments by ring-opening polymerization of ϵ-caprolactone using a catalytic amount of tin(II) 2-ethylhexanoate ($Sn(Oct)_2$) with controlled monomer-to-initiating hydroxyl group molar ratio ($[\epsilon\text{-CL}]_0/[-OH]_0$) and were followed by hydrogenolysis under a hydrogen (H_2) atmosphere using a palladium on activated carbon (Pd/C, 5 wt % Pd) catalyst to produce α-carboxylic-ω-dihydroxy AB_2 macromonomers **3**, 2,2-bis[ω-hydroxyoligo(ϵ-caprolactone)methyl]propionic acid. Finally, HPCLs were prepared by polycondensation of **3** in the presence of *p*-toluenesulfonic acid (TSA) with continuous water removal. To investigate and compare the role of hyperbranched structure against conventional linear structure, linear poly(ϵ-caprolactone) (LPCL), whose chemical structure and molecular weight are similar to those of HPCLs, was commercially purchased and used as a linear counterpart of HPCLs.

2.2. Measurements. The chemical structures of synthesized materials were analyzed by ^{1}H NMR spectroscopy using a Bruker Avance DPX-300 spectrometer with the tetramethylsilane (TMS) proton signal as an internal standard in $CDCl_3$. ^{1}H NMR spectra were also analyzed to determine the average number of ϵ-caprolactone monomer units incorporated in **2**, $\langle N_{\epsilon-CL}\rangle$, the average number of the AB_2 macromonomer units incorporated in **4**, $\langle N_{AB_2}\rangle$, and consequently the number-average molecular weights of **4**.

A Mettler DSC-30 differential scanning calorimeter was used to investigate the overall kinetics of nonisothermal crystallization of HPCLs and LPCL. The samples were heated to 100 °C under dry nitrogen gas to suppress the thermal oxidation and kept for 3 min to eliminate thermal history. Nonisothermal crystallization was performed by a controlled cooling of the aforementioned melt samples at different cooling rates, ranging from 2 to 10 °C/min.

Steady-shear viscosity measurements were performed on a TA Instruments AR 2000 constant-stress rheometer using a cone-and-plate geometry with a 2° angle and 6 cm diameter cone. The temperature was controlled by a Peltier lower plate with a precision of 0.1 °C, and the measurements were performed at regular intervals of 10 °C ranging from 60 to 120 °C. To minimize the effect of the thermal expansion of the rheometer, the gap between the cone and the plate was automatically controlled at all temperatures to 56 μm. The range of shear rate measured was from 0.1 to 100 s^{-1}.

A Leica MPS30 polarized optical microscope equipped with a Mettler Toledo FP82HT hot stage and a Mettler Toledo FP90 controller was used to observe the crystal morphology developed and the spherulites growth behavior during the isothermal process. The samples were first melted and kept on one hot stage at 100 °C for 3 min and then rapidly transported to another hot stage equipped in optical microscope and controlled at the crystallization temperature of 40 °C. The digital images were taken at desired crystallization times and further analyzed using a homemade image processor to calculate the average sizes of the growing spherulites.

Scheme 1

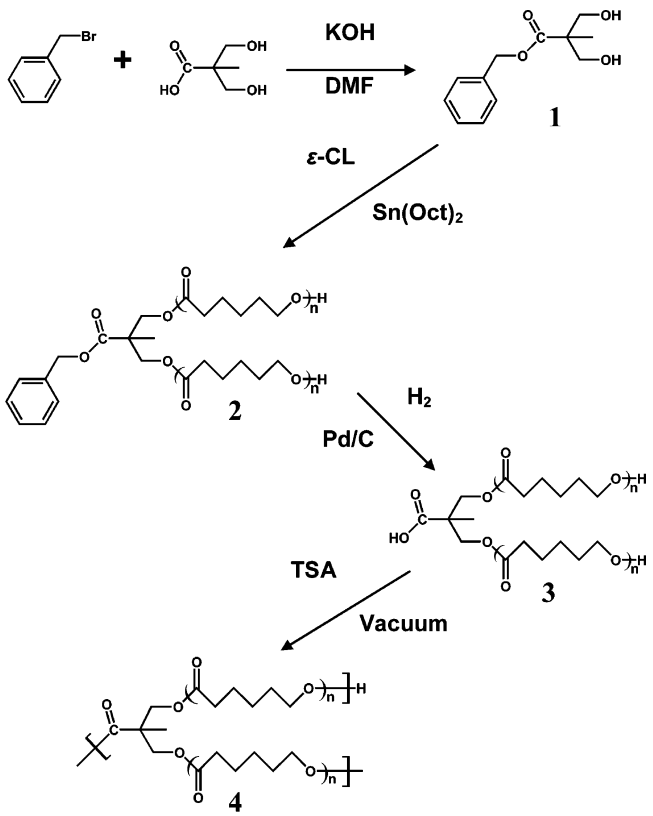

3. Results and Discussion

3.1. Synthesis and Molecular Architectural Characterization. Hyperbranched poly(ϵ-caprolactone)s (HPCLs) **4** were synthesized according to a reaction first developed by Trollsås et al.[19] and recently modified in our previous study, in which HPCLs had been prepared by polycondensation of the AB_2 macromonomers **3** with continuous removal of water[25] (Scheme 1).

The AB_2 macromonomers were prepared to incorporate the three different lengths of homologous oligo(ϵ-caprolactone) segments by ring-opening polymerization

Table 1. General Characteristics and Schematic Drawings of Hyperbranched Poly(ϵ-caprolactone)s and Their Linear Counterparts

Sample	AB_2 macromonomer Entry	$[\epsilon\text{–CL}]_0/[\text{–OH}]_0$[a]	$\langle N_{\epsilon\text{-CL}}\rangle$[b]	$\langle N_{AB_2}\rangle$[c]	M_n[d]	M_w/M_n[d]	Sample
HPCL–5	AB_2–5	5	5.7	8.1	11,800	1.8	
	AB_2–10	10	10.3	5.1	12,600	1.6	HPCL–10
HPCL–20	AB_2–20	20	20.1	3.3	15,700	1.5	
	·	·	·	·	10,700	1.4	LPCL[e]

[a] ϵ-Caprolactone monomer-to-initiating hydroxyl group molar ratio. [b] Average number of ϵ-caprolactone units incorporated in AB_2 macromonomers determined by ^{1}H NMR. [c] Average number of the AB_2 macromonomer units incorporated in HPCLs determined by ^{1}H NMR. [d] Obtained from SEC-MALLS. [e] Linear poly(ϵ-caprolactone) (Aldrich Chemicals).

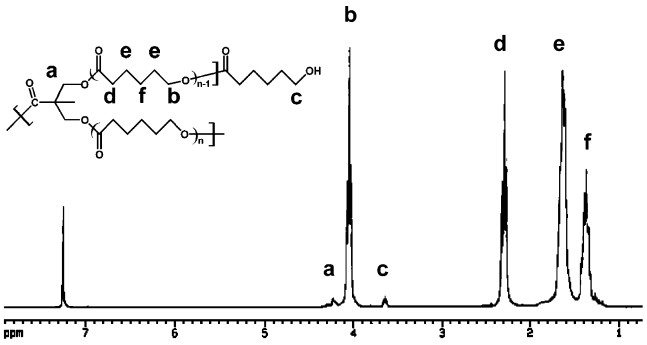

Figure 1. ^{1}H NMR spectrum (300 MHz) of hyperbranched poly(ϵ-caprolactone) (HPCL-10).

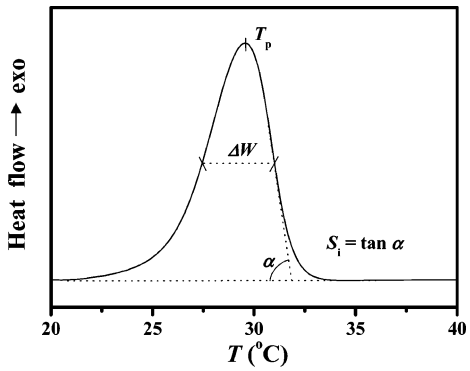

Figure 2. Schematic representation of all crystallization parameters during nonisothermal process.

with various ϵ-caprolactone-to-initiating hydroxyl group molar ratio ($[\epsilon\text{-CL}]_0/[-\text{OH}]_0$ = 5, 10, and 20, respectively) followed by hydrogenolysis deprotection and accordingly referred to as AB_2-5, -10, and -20, respectively. Thus, HPCLs were prepared to have intrinsically different lengths of branches and/or repeating backbone segments by the utilizing different AB_2 macromonomers and accordingly referred to as HPCL-5, -10, and -20, respectively. The average number of ϵ-caprolactone monomer units incorporated in the AB_2 macromonomers, $\langle N_{\epsilon-\text{CL}}\rangle$, indicating the length of linear oligomeric backbone segments, was calculated from the ratio of the integrated area of the peak corresponding to the repeating methylene units ($-\text{CO}CH_2$, δ 2.22) to the integrated area of the peak corresponding to the chain ends ($-CH_2\text{OH}$, δ 3.59) in ^{1}H NMR spectra of the AB_2 macromonomers, and in a similar manner, the average number of the AB_2 macromonomer units incorporated in HPCLs, $\langle N_{AB_2}\rangle$, was calculated from the following equation based on the branching theories developed by Flory:[26] $\langle N_{AB_2}\rangle = m/\{2\langle N_{\epsilon-\text{CL}}\rangle - m\}$, where m represents the ratios of the integrated area of the peak corresponding to the repeating methylene units (Figure 1, d) to the integrated area of the peak corresponding to the chain ends (Figure 1, c) of HPCLs. Here, it is worthy to note that the average number of branching points existing in HPCLs is equal to the value $\langle N_{AB_2}\rangle - 1$.

Listed in Table 1 are the general characteristics of three HPCLs and their linear counterpart, LPCL, along with the schematic drawings of HPCL molecules and LPCL molecule. The average length of oligo(ϵ-caprolactone) segments in these molecules, and the average numbers of macromonomers in hyperbranched molecules were determined to be $\langle N_{\epsilon-\text{CL}}\rangle$ and $\langle N_{AB_2}\rangle$ based on the assumption that the reactivities of B parts in the AB_2 macromonomers are equal, which in turn caused macromonomers to be randomly incorporated.

The molecular architectural variations among HPCLs and LPCL in the present study, which are well reflected in Table 1, are that in the order of HPCL-5, -10, and -20, the lengths of linear oligo(ϵ-caprolactone) segments appear to increase in length and the numbers of branching points in HPCL molecules decrease in number, while LPCL is made of one long linear chain of poly(ϵ-caprolactone).

3.2. Nonisothermal Crystallization Kinetics. Figure 2 shows a typical DSC curve for the nonisothermal crystallization process during cooling from the melt.

As shown in this figure, following useful parameters can be obtained to describe the nonisothermal crystallization behavior of samples: (1) the peak temperature, T_p; (2) the initial slope of the exotherm at inflection on the high-temperature side, S_i; (3) the width at half-height of the exothermic peak, ΔW.[27–30] Figure 3 exhibits the exothermic curves during the nonisothermal crystallization for HPCL-5, HPCL-10, HPCL-20,

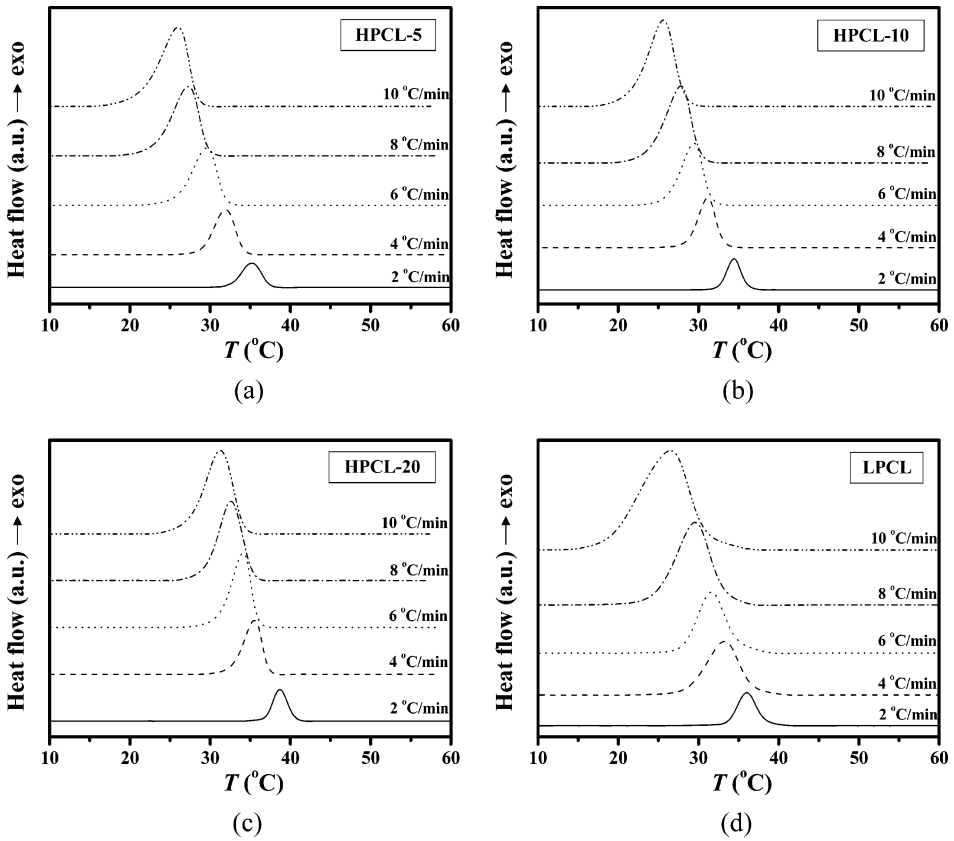

Figure 3. Nonisothermal crystallization exotherms of the HPCL-5 (a), HPCL-10 (b), HPCL-20 (c), and LPCL (d) measured at various cooling rates.

Table 2. Crystallization Parameters of Hyperbranched Poly(ϵ-caprolactone)s and Their Linear Counterparts

sample	crystallization parameter	cooling rate (°C/min) 2	4	6	8	10
HPCL-5	T_p (°C)	35.2	32.0	29.6	27.3	25.0
	S_i	0.54	0.68	0.83	0.91	1.02
	ΔW (°C)	2.8	3.1	3.5	3.8	4.1
	ΔH_c (J/g)	73.0	71.8	70.8	67.7	67.1
	X_c (%)	53.5	52.7	51.9	49.6	49.2
HPCL-10	T_p (°C)	35.4	31.2	29.4	27.8	25.6
	S_i	0.65	0.72	0.86	0.91	1.20
	ΔW (°C)	2.1	2.6	3.1	3.7	3.9
	ΔH_c (J/g)	79.1	77.4	76.1	75.4	72.2
	X_c (%)	58.0	56.8	55.8	55.3	52.9
HPCL-20	T_p (°C)	38.7	35.5	34.1	32.6	31.2
	S_i	0.78	0.91	1.03	1.21	1.45
	ΔW (°C)	2.1	2.7	2.8	3.4	4.1
	ΔH_c (J/g)	82.9	82.2	80.6	78.8	73.8
	X_c (%)	60.7	60.2	59.1	57.8	54.1
LPCL	T_p (°C)	36.0	33.2	31.6	29.6	26.4
	S_i	0.75	0.79	0.94	1.18	1.23
	ΔW (°C)	2.7	4.6	2.9	4.9	7.1
	ΔH_c (cal/g)	80.2	78.2	77.2	75.3	73.0
	X_c (%)	58.8	57.3	56.6	55.2	53.5

and LPCL at various cooling rates ranging from 2 to 10 °C/min.

All DSC curves shown in Figure 3 were analyzed to calculate the above-mentioned crystallization parameters, and the results are summarized in Table 2. The experimental errors were examined with at least five runs for each sample at each cooling rate under precisely controlled condition. The parameters T_p, S_i, and ΔW listed in Table 2 were found to be reproducible to ±1 °C, ±0.1, and ±2 °C, respectively. It is clearly seen in Figure 3 that T_p shifted to lower temperatures for all samples as the cooling rate increased, indicating the increase in supercooling. On the other hand, for a given cooling rate, T_p for each HPCL shifted to a high-temperature region with the increase in the length of the incorporated linear backbone segments and the decrease in the number of branching point. This indicates acceleration of crystallization temperature caused by the incorporation of the longer linear crystallizable oligo(ϵ-caprolactone) segments onto HPCL backbone. T_p for LPCL was observed in the region between HPCL-10 and HPCL-20 for a given cooling rate, the origin of which will be discussed in detail in a later section. The S_i of the curves in Figure 3 was employed to express relative kinetics of the nonisothermal crystallization process.[27−30] Higher absolute values of the initial slope, suggesting faster crystallization, were assigned to HPCL with the longer linear backbone segments and fewer number of branches. On the other hand, the absolute value of S_i for LPCL at a given cooling rate was between those of HPCL-10 and HPCL-20, indicating that crystallization rate of LPCL mediates between HPCL-10 and HPCL-20.

As indicated in Table 2, the cooling rate also had a profound effect on the crystallization kinetics. The crystallization was faster for higher cooling rates, suggesting the nucleation-dominated process as dictated in many previous literatures. The ΔW is a measure of the distribution of the crystal dimensions; i.e., the smaller the ΔW, the narrower the distribution.[28−30] From ΔW values calculated in Table 2, it was found that the distributions of the crystal dimensions for HPCL-5 and HPCL-10 are slightly broader than HPCL-20, which might be the result of the slower crystallization rate and little broader molecular weight distribution as

indicated in Table 1. In addition, the crystallinity, X_c, of all samples were calculated using the following formula

$$X_c\,(\%) = \frac{\Delta H_c}{\Delta H_{100}} \times 100 \qquad (1)$$

where ΔH_c is the heat of crystallization of the sample and ΔH_{100} is the heat of crystallization for a 100% crystalline poly(ϵ-caprolactone), which is taken as 136.4 J/g.[31] The ΔH_c and corresponding X_c of HPCLs and LPCL are also summarized in Table 2. Among HPCLs, the X_c calculated for a given cooling rate increased with the longer linear backbone segments and the fewer branches in the molecules, whereas the X_c of LPCL is in the middle of HPCL-10 and HPCL-20. To investigate the nonisothermal crystallization kinetics in detail and more quantitatively, the measured nonisothermal crystallization exotherms in Figure 3 were further analyzed by the modified Avrami method.

Integration of the exothermal peaks during the nonisothermal scan gives relative crystallinity, X_t, as a function of temperature, which can be transformed into a function of time:[32,33]

$$X_t = \frac{\int_0^t (dH_c/dt)\,dt}{\int_0^\infty (dH_c/dt)\,dt} \qquad (2)$$

Here, t_0 and t_∞ denote the onset and completion time of crystallization, respectively, and dH_c/dt is the rate of heat evolution. Figure 4 shows the X_t variations as a function of crystallization time for HPCLs and LPCL. As seen in Figure 4, the lower the cooling rate, the larger the time range at which crystallization occurs. In addition, all curves are seen to have approximately the same reverse S-shape, indicating that only the retardation effect of cooling rate on the crystallization can be observed in these curves.[34,35]

On the basis of the assumption that the crystallization temperature is constant, the classical Avrami equation was used for describing the primary stage of the nonisothermal crystallization kinetics.[32,36−38] In this case, the Avrami equation can be expressed as follows

$$X_t = 1 - \exp[-Kt^n] \qquad (3)$$

where K is the rate constant containing the nucleation and the growth parameter in the nonisothermal crystallization process, and n is the Avrami exponent whose values depend on the mechanism of nucleation and on the nature of crystal growth.[39−41] To facilitate the evaluation of the Avrami parameters (n and K), the double-logarithmic form is often taken to rearrange eq 3 as follows:

$$\log[-\ln(1 - X_t)] = \log K + n \log t \qquad (4)$$

Figure 5 shows the $\log[-\ln(1 - X_t)]$ vs $\log t$ plots, so-called Avrami plots, for HPCLs and LPCL. It is shown in Figure 5 that the Avrami plots for the nonisothermal crystallization of HPCLs and LPCL vary linearly with one slope in a relatively large range of crystallization time, though a slight deviation from the straight line derived in the middle of the curves is also observed at both ends of the curves. From the slope and the intercept of the straight lines, the Avrami exponents and

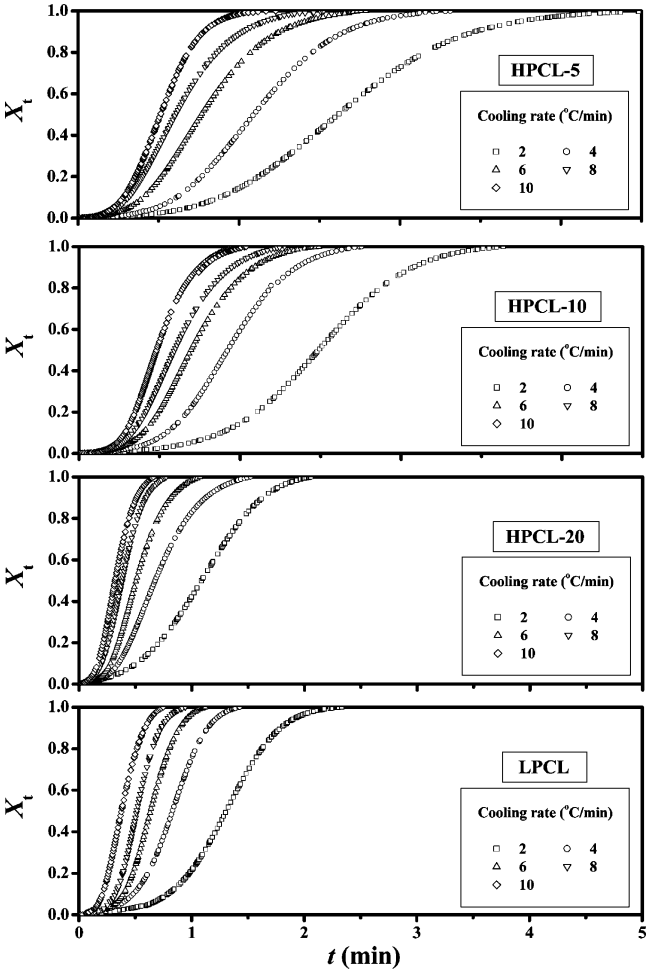

Figure 4. Plots of relative crystallinity, X_t, vs crystallization time, t, of HPCLs and LPCL.

the rate constants for HPCLs and LPCL were estimated, respectively, and listed in Table 3. The derived Avrami exponents for HPCLs and LPCL, ranging from 2.4 to 3.3 as listed in Table 3, were not affected much by either the cooling rate or the molecular architecture of samples. The Avrami exponents in this range are known to be obtained with various combinations of heterogeneous vs homogeneous nucleation, dimensionality of growth, and diffusion-restricted vs non-diffusion-restricted growth.[27,42] However, obtaining further insight into the nucleation and crystal growth mechanism with these Avrami exponents is not within the scope of research which is focused more on the crystallization kinetic rate constants and its correlation with the molecular architecture for HPCLs.

Here, it is worthy to note that the K values in Table 3 are inadequate to characterize the nonisothermal crystallization kinetics due to the influence of the cooling rate and should be corrected adequately. Assuming that the cooling rate is constant or approximately constant, the final form of the kinetic rate constant, K_c, can be given by the following correction:[35,43,44]

$$\log K_c = \frac{\log K}{\chi} \qquad (5)$$

The corrected rate constants for HPCLs and LPCL at various cooling rates are shown in Figure 6. Among the HPCLs at a given cooling rate, the K_c values are seen to increase with the increase in the lengths of linear

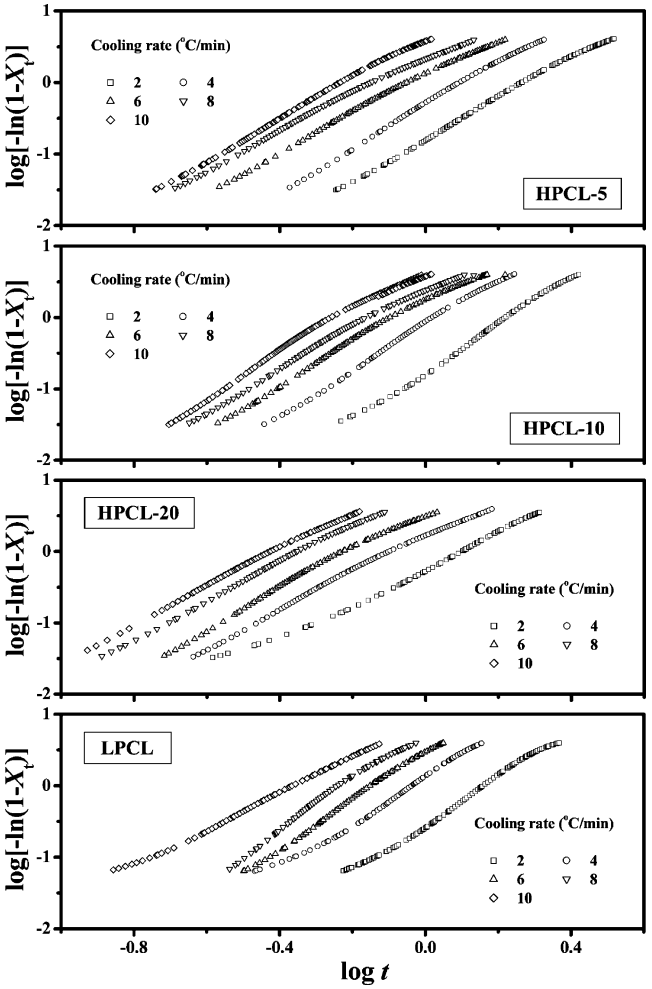

Figure 5. Plots of $\log[-\ln(1 - X_t)]$ vs $\log t$ for HPCLs and LPCL.

backbone segments and the decrease in the number of branches, which are HPCL-5 < HPCL-10 < HPCL-20. On the other hand, the K_c of LPCL showed an intermediate value between those of HPCL-10 and HPCL-20.

In addition, the crystallization half-time, $t_{1/2}$, defined as the time at which the extent of crystallization is complete by 50%, was determined from the derived K_c and n as follows[35,43−45]

$$t_{1/2} = \left(\frac{\ln 2}{K_c}\right)^{1/n} \tag{6}$$

and are also listed in Table 3. Considering that the reciprocal of $t_{1/2}$ corresponds to the overall crystallization rate, the result of the overall crystallization rate for HPCLs and LPCL was in good agreement with K_c result.

The overall crystallization of polymers can be envisaged as a two-step process: (1) the first step is the cooperative movement of polymer chains in parallel array, and (2) the second step is crystallization of these ordered chain occurring by means of intermolecular interactions with a concomitant decrease in free energy.[42] Commonly, hyperbranched polymers (HBPs), although they show a faster molecular motion, are known to be more amorphous compared to their linear counterpart having similar chemical backbone structure and molecular weight.[7−9] In the conventional HBPs, numerous branching points resulting from the use of

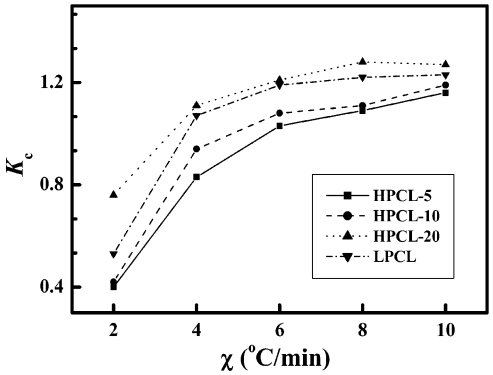

Figure 6. Corrected Avrami rate constant, K_c, for HPCLs and LPCL at various cooling rates.

Table 3. Values of Avrami Exponent, *n*, Rate Constant, *K*, the Corrected Rate Constant, K_c, and the Crystallization Half-Time, $t_{1/2}$, of Hyperbranched Poly(ϵ-caprolactone)s and Their Linear Counterparts at Various Cooling Rates

sample	modified Avrami analysis	cooling rate (°C/min) 2	4	6	8	10
HPCL-5	*n*	2.9	2.9	2.6	2.5	2.9
	K	0.16	0.47	1.19	1.99	4.41
	K_c	0.40	0.83	1.03	1.09	1.16
	$t_{1/2}$	1.21	0.94	0.86	0.83	0.84
HPCL-10	*n*	3.3	3.1	2.8	2.7	3.1
	K	0.18	0.78	1.59	2.30	5.69
	K_c	0.42	0.94	1.08	1.11	1.19
	$t_{1/2}$	1.16	0.91	0.85	0.84	0.84
HPCL-20	*n*	2.5	2.4	2.5	2.6	2.5
	K	0.58	1.52	3.14	7.21	10.92
	K_c	0.76	1.11	1.21	1.28	1.27
	$t_{1/2}$	0.96	0.82	0.80	0.79	0.78
LPCL	*n*	3.3	3.1	3.3	3.1	2.5
	K	0.28	1.31	2.84	4.91	7.93
	K_c	0.53	1.07	1.19	1.22	1.23
	$t_{1/2}$	1.08	0.87	0.85	0.83	0.80

the small AB_2 (or A_2B_2, AB_3, etc.) monomers in syntheses bring about imperfection of the chains, consequently deterring effective interaction and regular chain packing for crystallization. However, in the case of HPCLs, the incorporated linear oligo(ϵ-caprolactone) backbone segments were quite long, and the branching points existing in the backbone chain were only a few compared to those in the other types of typical HBPs.[18,19] These architectural features of HPCLs may help the polymer chains to interact more effectively and pack more regularly, which accommodates the crystallization more effectively. Moreover, we found that the molecular architectural differences in the length of incorporated linear segments and the number of branching points altered the kinetic rates of the nonisothermal crystallization of HPCLs. That is, the slower crystallization rate was observed for HPCLs with shorter linear segments and with more branches as verified from the K_c and $1/t_{1/2}$ in the nonisothermal crystallization for a given cooling rate (HPCL-5 < HPCL-10 < HPCL-20). These phenomena can be explained by the less favorable thermodynamic condition of the HPCLs with the shorter segments (HPCL-5 and HPCL-10) than the HPCLs with the longer segments (HPCL-20). It is evident that there exist more frequent heterogeneous branching points, which act as an obstacle in regular chain packing, in the backbone of the HPCLs with shorter segments. However, LPCL comprising one long linear poly(ϵ-caprolactone) chain, which can be considered as in the most favorable thermodynamic condition among the samples, showed slower crystallization than HPCL-20.

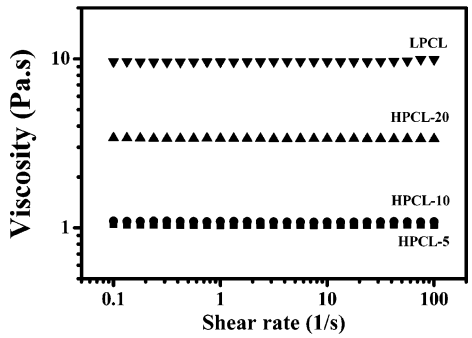

Figure 7. Steady shear viscosity as a function of shear rate for HPCLs and LPCL measured at 90 °C.

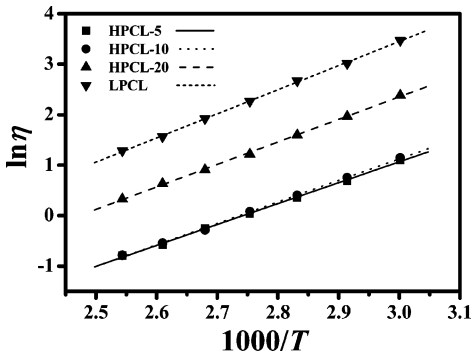

Figure 8. Temperature dependences of the viscosity for HPCLs and LPCL.

To understand the nature of the faster crystallization rate of HPCL-20 than LPCL, molecular motion of the samples in their melt state, which affects the first step of overall crystallization, was characterized by the measurement of steady shear melt viscosity (This will be discussed in the following section).

3.2. Steady Shear Melt Viscosity and Activation Energy of Flow. For HPCLs and LPCL, the viscosity was measured under steady shear in the temperature range 60−120 °C, where all samples are in their melt state. Figure 7 shows the exemplary results of steady shear viscosity for HPCLs and LPCL measured at 90 °C. For all HPCLs and LPCL, the viscosity was found to be independent of shear rate. This is characteristic of a Newtonian fluid.

The temperature dependences of the viscosity of HPCLs and LPCL are illustrated in Figure 8. From this figure, we can see that HPCLs and LPCL exhibit good linear relationships between ln η and $1/T$ within the temperature range employed, which is in good agreement with the kinetic rate theory of flow as represented by the Arrhenius−Frenkel−Eyring type equation as follows:[46]

$$\ln \eta = A + \frac{E_\eta}{RT} \tag{7}$$

The observed linearity of ln η vs $1/T$ relationships indicates that the apparent activation energy of flow, E_η, can be determined by the slopes of these plots. The derived E_η values for HPCLs and LPCL are summarized in Table 4. According to the kinetic theory of flow, the lower activation energy of flow corresponds to the faster cooperative diffusional motion of polymer chain.[47,48] As indicated in Table 4, the cooperative diffusional motion of polymer chains in their melt state is faster in the order of LPCL < HPCL-20 < HPCL-10 < HPCL-5.

Table 4. Activation Energy of Flow, E_η, and Spherulitic Radial Growth Rate, G, for Hyperbranched Poly(ϵ-caprolactone)s and Their Linear Counterparts

sample	HPCL-5	HPCL-10	HPCL-20	LPCL
E_η (kJ/mol)	34.4	35.4	37.1	39.8
G (μm/min)	1.5	4.9	15.3	11.4

Considering the overall crystallization as a two-step process, it is obvious that the polymer chains of HPCLs incorporating the shorter linear segments such as HPCL-5 and HPCL-10 can move faster than the polymer chains of HPCLs with the longer segments in parallel array to crystallize in the first step. However, many branching points existing in the HPCLs with the shorter segments act as an obstacle in the interaction and crystallization stage, as was explained in a previous section. On the other hand, it is worthy to bear in mind that HPCL-20 incorporates relatively long linear segments consisting or ca. 20 ϵ-caprolactone monomer units (ca. 120 carbons) and only a few branching points in the backbone, which can be considered as the thermodynamic condition acting in the later step of overall crystallization of HPCL-20, is almost as favorable as LPCL. Therefore, we could conclude that the polymer chains of HPCL-20 move faster in parallel array compared to those of LPCL in the first step of overall crystallization due to faster chain mobility in the melt state, which result in the faster crystallization rate as determined by the K_c and $1/t_{1/2}$.

3.3. Morphological Observation and Spherulite Radial Growth. Crystal morphology developed during melt quenched isothermal crystallization and radial growth behavior of spherulites was characterized using POM equipped with a hot stage. The morphological forms obtained under controlled nonisothermal conditions closely matched those reported for isothermal crystallization as in other works[27] and, hence, will not be presented here. POM images captured during isothermal crystallization of HPCLs and LPCL at 40 °C at various crystallization times are shown in Figure 9.

A characteristic pattern, which consists of a number of spherulites exhibiting a Maltase cross, as well as radial growth of spherulites with the crystallization time was observed for all samples. As seen in Figure 9, the number of growing crystals formed in the early stage of crystallization for each sample was found to be dependent on the molecular architecture as the number of nuclei formed is in the order of HPCL-20 > LPCL > HPCL-10 >HPCL-5. This phenomenon is correlated with the different molecular architectures of samples. Among HPCLs, the introduction of more branches in the backbone of molecules (HPCL-20 < HPCL-10 < HPCL-5) resulted in the decrease in chain regularity and the increase in steric hindrance, which slowed the formation of nuclei. Moreover, slower chain mobility of LPCL compared to HPCL-20 resulted in the fewer number of nuclei formed within the same crystallization time.

In Figure 10, the average radii of spherulites for HPCLs and LPCL are plotted against crystallization time. The radii of spherulites increase linearly with crystallization time up to the impingement of the spherulites. From the slopes of these lines, the spherulitic radial growth rate during the isothermal process, G, for HPCLs and LPCL was evaluated and are listed in Table 4. As indicated in Table 4, the trend of G values is in good agreement with the nonisothermal crystal-

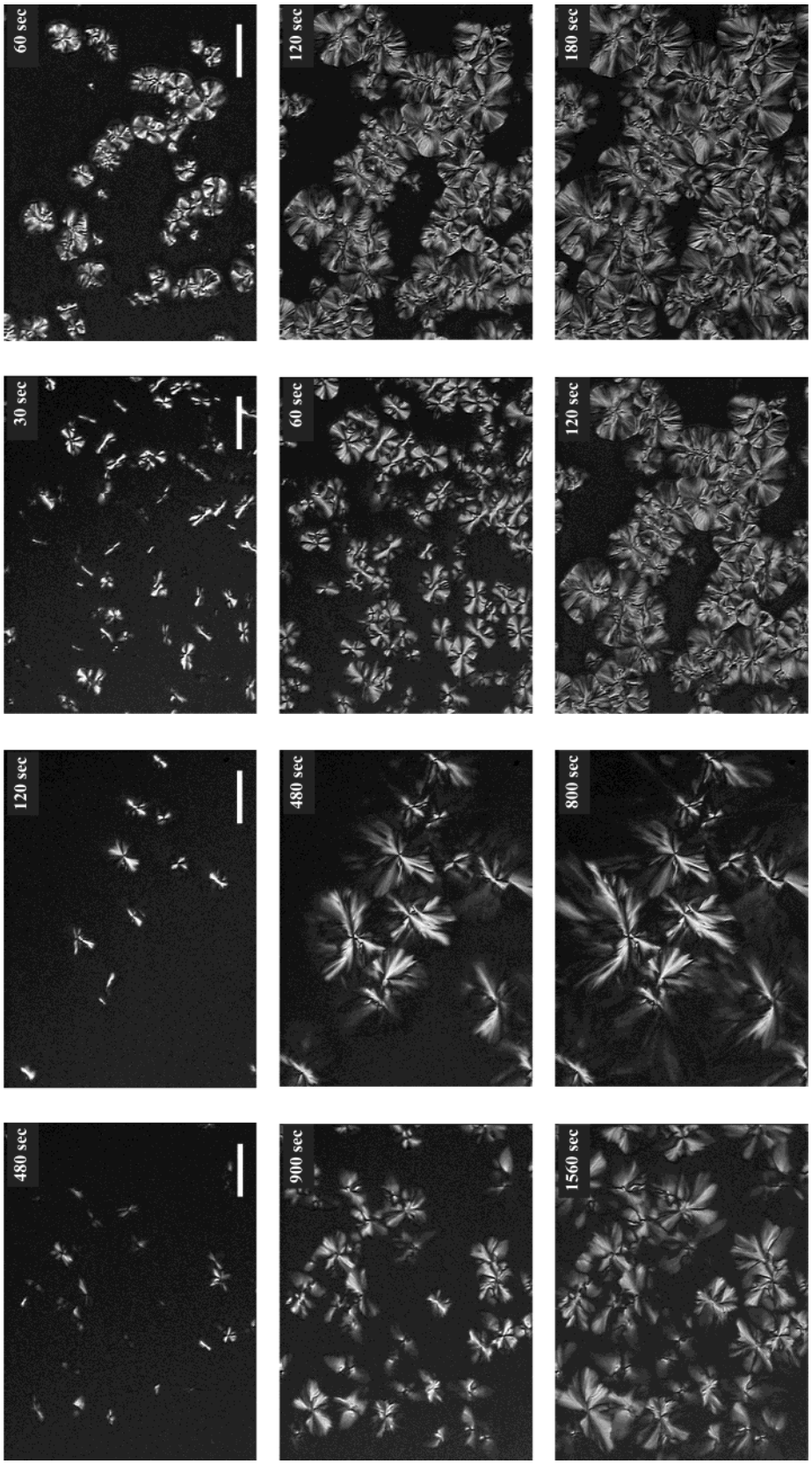

Figure 9. Polarized optical micrographs for HPCL-5 (a), HPCL-10 (b), HPCL-20 (c), and LPCL (d) crystallized at 40 °C from the melt after indicated crystallization time. The white bars correspond to 50 μm.

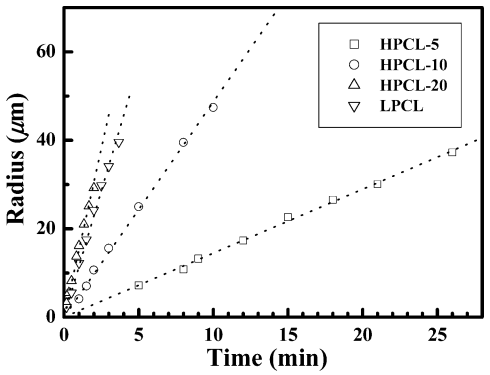

Figure 10. Variation in the spherulite radius with crystallization time for HPCLs and LPCL.

lization rate determined by the K_c and $1/t_{1/2}$ in the previous section.

4. Conclusions

In the present study, three hyperbranched poly(ϵ-caprolactone)s (HPCL-5, HPCL-10, HPCL-20) with the molecular architectural variation, which are the different lengths of homologous oligo(ϵ-caprolactone) segments and the different numbers of branching points, were prepared without significant changes in molecular weights, and linear poly(ϵ-caprolactone) (LPCL) whose chemical structure and molecular weight are similar to those of HPCLs was purchased and used as the linear counterpart. From the molecular architectural characterization performed by ^{1}H NMR end-group analyses, the lengths of the linear backbone segments were found to be in the increasing order of HPCL-5 < HPCL-10 < HPCL-20 by their $\langle N_{\epsilon-CL}\rangle$ values, and the numbers of branching points existing in the HPCL molecules were found to be in decreasing order of HPCL-5 > HPCL-10 > HPCL-20 by their $\langle N_{AB_2}\rangle$ values. Recognizing that LPCL consists of one long linear chain, it is evident that the length of the linear segments is the longest and the number of branching points is the smallest among the samples employed in this study.

The nonisothermal crystallization exotherms of the HPCLs and LPCL were measured by DSC at various cooling rates ranging from 2 to 10 °C/min. During the controlled cooling from the melt, the HPCLs with longer linear segments and fewer branches experienced faster crystallization; i.e., the initial slope in the exotherms at a given rate was higher. The nonisothermal crystallization kinetics was further investigated by the modified Avrami analyses. The Avrami exponents were determined to range from 2.4 to 3.3 regardless of the HPCLs and LPCL, which indicates that the nucleation and growth mechanism was not significantly influenced by the architectural variation. However, the nonisothermal crystallization rate constant, K_c, and the reciprocal of crystallization half-time, $1/t_{1/2}$, were found to be affected by the molecular architecture; the K_c and $1/t_{1/2}$ resulted in the order of HPCL-5 < HPCL-10 < LPCL < HPCL-20. The crystallization rate as characterized by K_c and $1/t_{1/2}$ was increased with the increase in the length of linear segments and the decrease in the branching point among the HPCLs. This phenomenon is assumed to be connected to the more frequent presence of chain heterogeneity in the case of the HPCLs with the shorter linear segments and greater number of branches. These heterogeneous branching points are expected to hinder the polymer chains from packing regularly for the effective crystallization. However, the slower crystallization rate of LPCL compared to that of the HPCL-20 was an unexpected behavior from the above-mentioned point of view because LPCL consisted of only one long chain with no chain heterogeneity. Steady shear melt viscosity measurements performed at various temperatures revealed that the cooperative chain mobility of the HPCL-20 is higher than that of LPCL in their melt state, indicating a faster ordering of polymer chains to further crystallize in the first step of overall crystallization. In addition, the linear segments incorporated in the HPCL-20 are relatively long such that thermodynamic condition for crystallization of ordered chains in parallel array in the second step could be nearly equivalent to that of LPCL, causing the overall crystallization of the HPCL-20 to occur at a faster rate than LPCL. From the morphological observation during isothermal crystallization at 40 °C, a number of spherulites exhibiting a Maltase cross were observed for all samples. Moreover, the average radii of spherulites increased linearly with isothermal crystallization time, and the derived radial spherulites growth rates for the HPCLs and LPCL were found to be in good agreement with the K_c and $1/t_{1/2}$ results that were estimated from the controlled nonisothermal processes.

Acknowledgment. The authors are grateful to the Ministry of Environment, Republic of Korea, for their support of this study through the Eco-Technopia 21 project. The authors also wish to express their gratitude to Sang-Wook Chun for performing DSC experiments.

References and Notes

(1) Fréchet, J. M. J. *Science* **1994**, *263*, 1710.
(2) Hedrick, J. L.; Miller, R. D.; Hawker, C. J.; Carter, K. R.; Volksen, W.; Yoon, D. Y.; Trollsås, M. *Adv. Mater.* **1998**, *10*, 1049.
(3) Fréchet, J. M. J.; Hawker, C. J.; Wooley, K. L. *J. Mater. Sci.: Pure Appl. Chem.* **1994**, *A31*, 1627.
(4) Denkewalter, R. G.; Kolc, J.; Lukasavage, W. J. U.S. Patent 4289872, 1981.
(5) Uhrich, K. E.; Hawker, C. J.; Fréchet, J. M. J. *Macromolecules* **1992**, *25*, 4583.
(6) Miller, T. M.; Neenan, T. X.; Kwock, E. W.; Stein, S. M. *J. Am. Chem. Soc.* **1993**, *115*, 356.
(7) Hawker, C. J.; Farrington, P. J.; Mckay, M. E.; Wooley, K. L.; Fréchet, J. M. J. *J. Am. Chem. Soc.* **1995**, *117*, 4409.
(8) Mourey, T. H.; Turner, S. R.; Rubinstein, M.; Fréchet, J. M. J.; Hawker, C. J.; Wooley, K. L. *Macromolecules* **1992**, *25*, 2401.
(9) Kim, Y. M.; Kim, Y. G. *J. Ind. Eng. Chem.* **1999**, *5*, 74.
(10) Kwak, S.-Y.; Lee, H. Y. *Macromolecules* **2000**, *33*, 5536.
(11) Kwak, S.-Y.; Ahn, D. U. *Macromolecules* **2000**, *33*, 7557.
(12) Hawker, C. J.; Lee, R.; Fréchet, J. M. J. *J. Am. Chem. Soc.* **1991**, *113*, 4583.
(13) Percec, V.; Kawasumi, M. *Macromolecules* **1992**, *25*, 3843.
(14) Johanssom, M.; Malmström, E.; Hult, A. *J. Polym. Sci., Polym. Chem.* **1993**, *31*, 619.
(15) Turner, S. R.; Voit, B. I.; Mourey, T. H. *Macromolecules* **1993**, *26*, 4617.
(16) Kricheldorf, H. R.; Lohden, G. *Macromol. Chem. Phys.* **1995**, *196*, 1839.
(17) Hawker, C. J.; Chu, F.; Pomery, P. J.; Hill, D. J. T. *Macromolecules* **1996**, *29*, 3831.
(18) Trollsås, M.; Atthoff, B.; Claesson, H.; Hedrick, J. L. *Macromolecules* **1998**, *31*, 3439.
(19) Trollsås, M.; Hedrick, J. L. *Macromolecules* **1998**, *31*, 4390.
(20) Long, Y.; Sharks, R. A.; Stachurski, Z. H. *Prog. Polym. Sci.* **1995**, *20*, 651.
(21) Keller, A.; Lester, G. R.; Morgan, C. B. *Philos. Trans. R. Soc.* **1954**, *A247*, 1.
(22) Di Lorenzo, M. L.; Silvestre, C. *Prog. Polym. Sci.* **1999**, *24*, 917.

(23) Tadmor, Z.; Gogos, C. G. *Principles of Polymer Processing*; John Wiley and Sons: New York, 1979.
(24) Ziabicki, A. *Fundamentals of Fiber Formation*; Wiley: London, 1976.
(25) Choi, J.; Kwak, S.-Y. *Macromolecules* **2003**, *36*, 8630.
(26) Flory, P. J. *J. Am. Chem. Soc.* **1952**, *75*, 2718.
(27) Andjelić, S.; Richard, R. E. *Macromolecules* **2001**, *34*, 896.
(28) Chen, C.; Fei, B.; Peng, S.; Zhuang, Y.; Dong, L.; Feng, Z. *Eur. Poym. J.* **2002**, *38*, 1663.
(29) Gupta, A. K.; Gupta, V. B. *J. Appl. Polym. Sci.* **1982**, *27*, 4669.
(30) Beck, H. N.; Ledbetter, H. D. *J. Appl. Polym. Sci.* **1965**, *9*, 2131.
(31) Crescenzi, V.; Manzini, G.; Calzolari, G.; Borri, C. *Eur. Polym. J.* **1972**, *8*, 449.
(32) De Juana, R.; Jauregui, A.; Calahorra, E.; Cortazar, M. *Polymer* **1996**, *37*, 3339.
(33) Ziabicki, A. *Appl. Polym. Symp.* **1967**, *6*, 1.
(34) Weng, W.; Chen, G.; Wu, D. *Polymer* **2003**, *44*, 8119.
(35) Liu, X.; Wu, Q. *Eur. Polym. J.* **2002**, *38*, 1383.
(36) Jeziorny, A. *Polymer* **1978**, *19*, 1142.
(37) Cebe, P. *Polym. Compos.* **1988**, *9*, 271.
(38) Herrero, C. H.; Acosta, J. L. *Polym. J.* **1994**, *26*, 786.
(39) Avrami, M. *J. Chem. Phys.* **1939**, *7*, 1103.
(40) Avrami, M. *J. Chem. Phys.* **1940**, *8*, 212.
(41) Wunderlich, B. *Macromolecular Physics*; Academic Press: New York, 1976; Vol. 2.
(42) Mandelkern, L. *Crystallization of Polymers*; McGraw-Hill: New York, 1963.
(43) Lee, S. W.; Lee, B.; Ree, M. *Macromol. Chem. Phys.* **2000**, *201*, 453.
(44) Lee, S. W.; Ree, M.; Park, C. E.; Jung, Y. K.; Park, C.-S.; Jin, Y. S.; Bae, D. C. *Polymer* **1999**, *40*, 7137.
(45) Shiomi, T.; Takeshita, H.; Kawaguchi, H.; Nagai, M.; Takenaka, K.; Miya, M. *Macromolecules* **2002**, *35*, 8056.
(46) Glasstone, S.; Laidler, K. J.; Eyring, H. *The Theory of Rate Processes*; McGraw-Hill: New York, 1941.
(47) Bailey, R. T.; North, A. M.; Pethrick, R. A. *Molecular Motion in High Polymers*; Oxford University Press: New York, 1981.
(48) Crank, J.; Park, G. S. *Diffusion of Polymers*; Academic Press: London, 1968.

MA035387F